crystals

MDPI

Article

Effect of Processing Technique Factors on Structure and Photophysical Properties of Perovskite Absorption Layer by Using Two-Step Spin-Coating Method

Zixiao Zhou [1], Xiaoping Zou [1,*], Jialin Zhu [1,*], Jin Cheng [1], Haiyan Ren [1], Chuangchuang Chang [1], Yujun Yao [1], Dan Chen [2,3], Xing Yu [1], Guangdong Li [1], Junqi Wang [1] and Baoyu Liu [1]

[1] Beijing Advanced Innovation Center for Materials Genome Engineering, Research Center for Sensor Technology, Beijing Key Laboratory for Sensor, MOE Key Laboratory for Modern Measurement and Control Technology, School of Applied Sciences, Beijing Information Science and Technology University, Jianxiangqiao Campus, Beijing 100101, China; 18049217206@163.com (Z.Z.); chengjin@bistu.edu.cn (J.C.); yanh3100@gmail.com (H.R.); changcc037@gmail.com (C.C.); yyj10zy@gmail.com (Y.Y.); nimingyx1@163.com (X.Y.); lgd1511455720@163.com (G.L.); 13126706081@163.com (J.W.); liubaoyu0214@163.com (B.L.)

[2] State Key Laboratory on Integrated Optoelectronics, Institute of Semiconductors, Center of Materials Science and Optoelectronics Engineering, University of Chinese Academy of Sciences, Chinese Academy of Sciences, Beijing 100864, China; chendan1988@semi.ac.cn

[3] Center of Materials Science and Optoelectronics Engineering, University of Chinese Academy of Sciences, Beijing 100049, China

* Correspondence: xpzou2014@163.com (X.Z.); jlzhu@bistu.edu.cn (J.Z.); Tel.: +86-136-4105-6404 (X.Z.)

Received: 23 July 2020; Accepted: 28 August 2020; Published: 28 August 2020

Abstract: The investigation of crystal growth is crucial for us to improve the film quality and photophysical properties of $CH_3NH_3PbI_3$ ($MAPbI_3$). In the two-step spin-coating process, the crystal structure could be modulated by controlling the growth conditions of PbI_2 and CH_3NH_3I (MAI) layers. In this paper, the PbI_2 layer was treated with annealing under different times. A liquid–liquid diffusion (LLD) mechanism is proposed to modify the deposition of MAI precursor solution and enhance the flatness of organic–inorganic hybrid perovskite film. Furthermore, the perovskite films are prepared using different concentrations of MAI. The evolution process of perovskite structure is observed by modulating the concentration of MAI. The spin-coating of moderate MAI tends to form high quality $MAPbI_3$ films with enhanced absorption and carrier extraction capabilities. The high concentration of MAI would cause the perovskite phase transition, which provides a novel perspective to modulate the structure of organic–inorganic hybrid perovskite in the two-step spin-coating process, although it deteriorates the device performance.

Keywords: two-step spin-coating process; anneal; liquid–liquid diffusion; solution concentration; phase transition

1. Introduction

The past ten years have witnessed the rapid development of perovskite solar cells (PSCs) [1–4]. The perovskite material, as the light absorption layer of the solar cells, has received tremendous attention, due to its suitable band gap [5–7], long charge carrier diffusion lengths [8–10], and good light absorption capability [11]. Therefore, the preparation process for the perovskite layer plays a crucial role in the performance of solar cell devices [12].

Optimizing the process for the perovskite layer includes adopting a deposition method, changing annealing conditions, and adjusting solution concentration. The one-step method and two-step methods are the conventional solution-processed deposition methods for preparing $CH_3NH_3PbI_3$ film [13,14]. The devices obtained using the two methods both exhibit high conversion efficiency. However, it is easier to control deposition conditions and obtain films with uniform coverage when the two-step method is used. [12,15–17].

In recent years, the optimization of the preparation process for the perovskite layer and its photonic applications have been rapidly developed [18–20]. In 2016, researchers achieved the dispersion and intimate passivation of crystalline organic–inorganic perovskite (OIP) nanoparticles through a swelling–deswelling microencapsulation process for ultra-stable and highly luminescent polymer composite films [18]. In 2018, Dong et al. reported an in-situ catalyst-free method to prepare inorganic $CsPbBr_3$ perovskite nanorods, and the obtained polymer matrix (NRs-PM) exhibits excellent dimensional controllability, outstanding optical properties, and ultrahigh environmental stability [19]. Recently, Wu et al. evaluated the performance of solid-state lighting (SSL) and liquid-crystal displays (LCDs) through calculations and optimizations [20]. The optimization for the deposition process of the PbI_2 layer is the foundation for the preparation of high-quality organic–inorganic hybrid perovskite film in a two-step process. Therefore, the nucleation state and crystallization quality of the PbI_2 layer have a direct impact on the growth of the perovskite film. The effects of annealing time and temperature for PbI_2 on crystallinity and film quality of perovskite were investigated [21]. It was reported that formation of the porous structure was obtained due to the time-delay thermal annealing of the PbI_2 layer, which was conducive to its conversion to perovskite layer [22]. Moreover, the coated PbI_2 layer was soaked in MAI solution for different times, and the impact on perovskite morphology could be observed [23]. In these articles, the long delay or annealing time of PbI_2 layer were adopted to generate PbI_2 crystals with high crystallinity, which was conducive to improving the penetration of MAI solution and forming high quality perovskite films. However, our team found residual solvent of the PbI_2 layer was beneficial to the liquid–liquid diffusion of the MAI solution and PbI_2 solution, resulting in a high crystalline film [24].

The growth of CH3NH3PbI3 crystals is also strongly related to the concentration of CH_3NH_3I in the two-step method [25]. Im et al. observed that the cuboid size of perovskite decreased exponentially with the increase in trace MAI (from 6 mg/mL to 10 mg/mL). Similar research was also investigated by Sun et al. [26]. However, a different trend for the change of grain size was observed, which might be ascribed to the different annealing and deposition conditions. The next year, 10 mg/mL and 40 mg/mL MAI were compared in the fabrication of a perovskite layer [27]. Denser and more uniform film was obtained with high concentration of MAI, and the grain size became larger, obviously, similar to our sample with 53 mg/mL. The cubic structure was shown in the above-mentioned perovskite layers, prepared with two-step spin-coating method. Unlike the spin-coating method, the substrate coated with PbI2 was placed in an MAI solution with the dipping method, and the effects of different concentration and dipping time of MAI solution on crystalline structure and morphology were investigated [28]. A higher MAI concentration (70 mg/mL) was used in the dipping method, and the tetragonal crystal structure of perovskite was obtained. In addition, the longer reaction time of PbI_2 and MAI was adopted and the perovskite showed tetragonal crystal structure, indicating that the different deposition process would impact the structure of perovskite, which would provide a meaningful reference for our work [29].

In this article, the effect of annealing time for the PbI2 layer in the two-step spin-coating process on the quality of organic–inorganic hybrid perovskite film was investigated. We found the LLD of MAI solution and unannealed PbI_2 layer was conducive to forming films with flat coverage, and the rough film was obtained with liquid–solid diffusion (LSD). Then, concentration of the MAI solution was adjusted to investigate the morphology and the photophysical properties of various organic–inorganic hybrid perovskite layers. Different from previous researches, the high concentration of MAI was adopted. It could be observed that the PbI_2 grain crystals formed at the interface between the perovskite

layer and hole transport layer with a low concentration of precursor solution (53 mg/mL), while a high concentration (93 mg/mL) would result in phase transition of perovskite structure. Larger grain size and more uniform film were obtained with a moderate concentration of MAI (73 mg/mL), which would be helpful to optimize the preparation process for the perovskite layer.

2. Materials and Methods

2.1. Materials

Fluorine-doped tin dioxide (FTO, 8–9 Ω/square, 2.1 mm in thickness, 1.5 × 1.5 cm^2 in area, light transmittance >80%) conductive transparent glass was purchased from Yingkou OPV Tech New Energy Co., Ltd. (Yingkou, China). Acetone, ethanol, and isopropanol were purchased from Sinopharm Chemical Reagent Beijing Co., Ltd. (Beijing, China). Nickel oxide (NiO) solution was acquired from Shanghai MaterWin New Materials Co., Ltd. (Shanghai, China). The *N*,*N*-dimethyl formamide (DMF, ≥99.8%) and dimethyl sulfoxide (DMSO, ≥99.8%) were acquired from Alfa Aesar (China) Co., Ltd. (Shanghai, China). Methylammonium iodide (CH_3NH_3I/MAI, white powder, ≥99%) and lead (II) iodide (Pbl_2, yellow crystalline powder, ≥99%) were obtained from Xi'an Polymer Light Technology Corp. (Xi'an, China).

2.2. Device Fabrication

2.2.1. Cleaning of FTO Conductive Glass

First, a mixture solution of detergent and deionized water was added to the Petri dish, and the FTO glass substrate was dipped in the solution for ten min. The purpose is to remove impurities and grease on the surface of the substrate, which would improve the conductivity of the substrate. Then we placed the cleaned FTO substrate glass in a Petri dish with the conductive surface facing up. Detergent solution (volume ratio: acetone:isopropanol:deionized water = 1:1:1) was added to the Petri dish. Then, the Petri dish was placed in an ultrasonic cleaner to clean for 20 min. Ethanol was used to clean the FTO, according to the above method. Lastly, the dried FTO glass substrate was placed in the drawer type UV light cleaning machine, and treated with ultraviolet ozone for 15 min to eliminate organic impurities and improve its hydrophilicity.

2.2.2. Preparation of NiO_x Hole Transport Layer

NiO solution was stirred by temperature-control magnetic stirrer for 8 h. Then, the filtered solution was spin-coated on an FTO substrate at 4000 rpm for 30 s. Finally, the FTO/NiO_x substrate was annealed on a hot plate at 150 °C for 10 min, and the as-annealed NiO_x film was sintered at 350 °C for 1 h in a ceramic fiber muffle furnace (the rising time was set to be half an hour).

2.2.3. Preparation of Perovskite Thin Film

The experiment was divided into two sections. In the first part of the experiment, 0.5993 g (1.3 mmol) PbI_2 powder was dissolved into a mixture solution of DMSO and DMF (1 mL, volume ratio: 0.05:0.95) completely, and spin-coated on an FTO/NiO_x substrate at 1500 rpm for 30 s. Then, the FTO/NiO_x/PbI_2 samples were annealed on a hot plate at different times (0 s, 10 s, and 20 s), and the annealing temperature was 150 °C. Finally, 73 mg of MAI powder was dissolved in isopropanol solution (1 mL) completely, and spin-coated onto the PbI_2 film at 1500 rpm for 30 s. The formed films were annealed on a hot plate at 150 °C for 150 min. The annealing time of the PbI_2 layer (0 s) was selected in Section 2 of our experiment. The different weights of MAI powder (53 mg, 73 mg, and 93 mg) were dissolved in isopropanol solution (1 mL) completely, and spin-coated onto the PbI_2 film at 1500 rpm for 30 s. Then, the films were annealed on a hot plate at 150 °C for 15 min. All experiments were performed at room temperature in ambient condition.

2.3. Characterization

The morphology of organic–inorganic hybrid perovskite film was measured with a scanning electron microscope (SEM) (SIGMA, Zeiss, Jena, Germany). X-ray diffraction (XRD) data of perovskite layers deposited on FTO/NiO_x bottoms were measured with an X-ray diffractometer (D8 Focus, Bruker, Dresden, Germany). Absorption spectra of the perovskite films on FTO/NiO_x bottoms were measured with an ultraviolet–visible (UV–Vis) absorption spectrometer (Avantes, Apeldoom, The Netherlands), and a LabRAW HR800 photoluminescence (PL) testing system (HORIBA Jobin Yvon, Paris, France) was employed to obtain the photoluminescence (PL) spectroscopy data.

3. Results and Discussion

In the two-step preparation process, the various annealing times of the PbI_2 layer are investigated firstly. In our work, the coated PbI_2 layers were annealed for 0 s, 10 s, and 20 s, respectively. To ensure the reliability of the experiment, the MAI concentration of 73 mg/mL was selected. SEM images and enlarged images of perovskite films with different PbI_2 annealing times are shown in Figure 1. The unannealed condition of coated PbI_2 results in the retention of DMSO and DMF solution, which is conducive to the diffusion of MAI precursor solution. Therefore, the perovskite films with high surface flatness and denseness are obtained through liquid–liquid diffusion (Figure 1a,d). The increase in annealing time leads to the growth of PbI_2 solid, which reacts with deposited MAI solution to form organic–inorganic hybrid perovskite film with loose structure in the surface. Thin films with rough surface and a few voids are formed through two diffusion mechanisms (liquid–liquid and liquid–solid), as shown in Figure 1b,c,e,f.

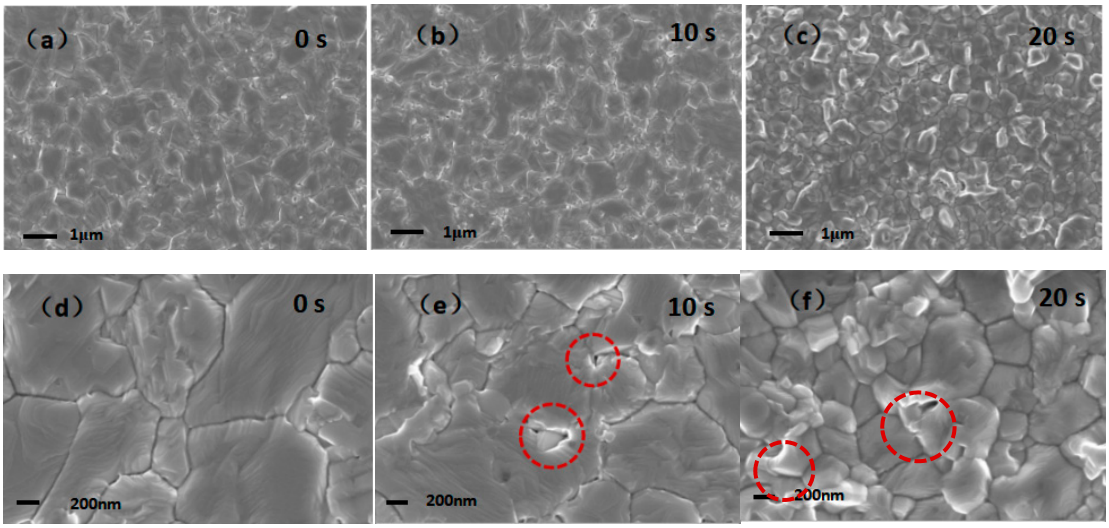

Figure 1. Top views of organic–inorganic hybrid perovskite films with different PbI_2 annealing time. (**a**–**c**) are top views of perovskite films annealed at 0 s, 10 s, and 20 s, and (**d**–**f**) are enlarged views of (**a**–**c**), respectively.

SEM cross-section views of organic–inorganic hybrid perovskite thin films prepared with 0 s, 10 s, and 20 s annealing time of PbI_2 layers are shown in Figure 2. With 0 s annealing of PbI_2, the interface of perovskite film and hole transport layer is flat with even coverage (Figure 2a). As the annealing time increases, the growth of irregular crystals can be observed at the interface (Figure 2b), resulting in the decrease in film flatness and thickness. More serious deterioration at the interface is shown in Figure 2c, which would lead to the increase in defect density. Overall, the poor interfaces of 10 s and 20 s annealing samples are due to the growth of PbI_2 crystals and loose structure formed through liquid–solid diffusion. Through the analysis of the morphology, it can be found that the annealing time

of the PbI_2 layer has an effect on the surface flatness of the perovskite film. The result is similar to the previous report of our group.

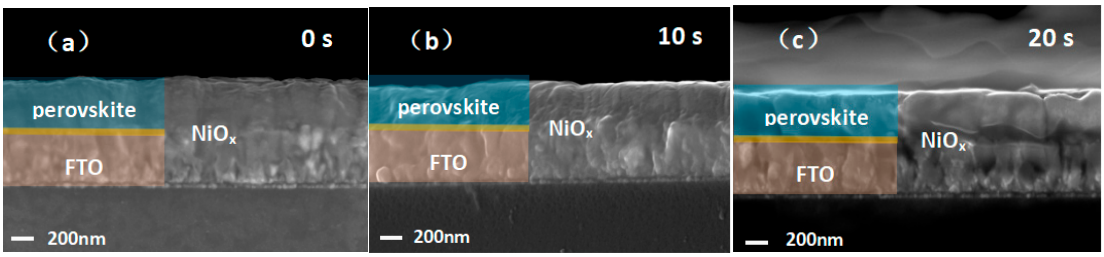

Figure 2. (**a**–**c**) Cross-sectional views of organic–inorganic hybrid perovskite films with different PbI_2 annealing times.

To illustrate the growth of perovskite films in detail, the evolution process of organic–inorganic hybrid perovskite films with different annealing conditions is shown in Figure 3. With 0 s annealing, DMF and DMSO solution is not completely volatilized. The contact between the MAI precursor solution (73 mg/mL) and the PbI_2 solution belongs to a liquid–liquid diffusion. It is easier for MAI solution to diffuse into the bottom layer, which is conducive to growing flat film. However, part of a solid PbI_2 crystal is formed on the topmost layer of the PbI_2 film with the annealing condition. With the deposition of MAI precursor solution, loose and uneven perovskite film is partially formed through liquid–solid diffusion (LSD) between precursor solution and the solid topmost layer of PbI_2. Therefore, the rough film is obtained, as shown in Figure 3, which is ascribed to the different contact mechanism and crystal growth rate of LLD and LSD between the MAI precursor solution and the PbI_2 layer. The adjustment of annealing mainly depends on the time and temperature. Studies have demonstrated that PbI_2 film with high crystallinity can be obtained under annealing conditions of high temperature for several minutes, and the MAPbI3 film retains a similar trend. However, in our optimized processing, the compact and flat perovskite film is formed on the liquid PbI_2 bottom layer.

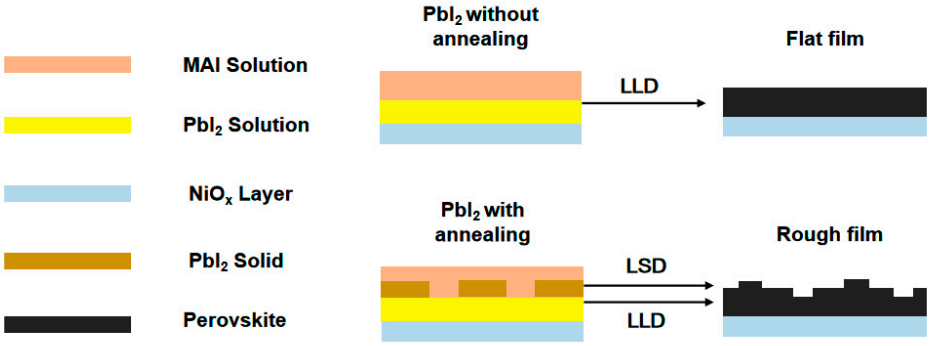

Figure 3. Evolution schematic diagram of organic–inorganic hybrid perovskite morphology with different annealing conditions.

In the two-step method, the morphology and photophysical properties of the light-absorbing layer can be controlled by the MAI concentration [25]. It is pointed out that the grain size and surface roughness of the perovskite layer are related to the concentration of MAI. In this part of the experiment, different concentrations of MAI are introduced, and the PbI_2 layer is not annealed, employing the previous optimization strategy. SEM top views and enlarged views of organic–inorganic hybrid perovskite films deposited with various concentration of MAI are shown in Figure 4a–f. The compact and smooth grains could be observed from Figure 4a,b, which is similar to the perovskite morphology reported in previous literature [27]; and there are small particles at the boundaries of cubic grains, which may be the residual PbI_2 crystals [30]. Large grain size and decrease in grain boundaries can be observed with the MAI concentration of 73 mg/mL (corresponding to Figure 4b,e). The grain

boundaries, as the recombination center of perovskite film, would reduce the device performance. As the concentration of the MAI solution increases to 93 mg/mL, the rough surface of the perovskite film is obtained, which is caused by the large area coverage of the dendritic structure grains and a lot of voids. A gradual process structural transition is demonstrated in Figure 4, indicating that the concentration of MAI precursor solution has a great impact on the growth of perovskite. The dendritic structure grains of Figure 4c are different to other samples significantly, which demonstrates the structural deterioration under excessively high concentrations of MAI.

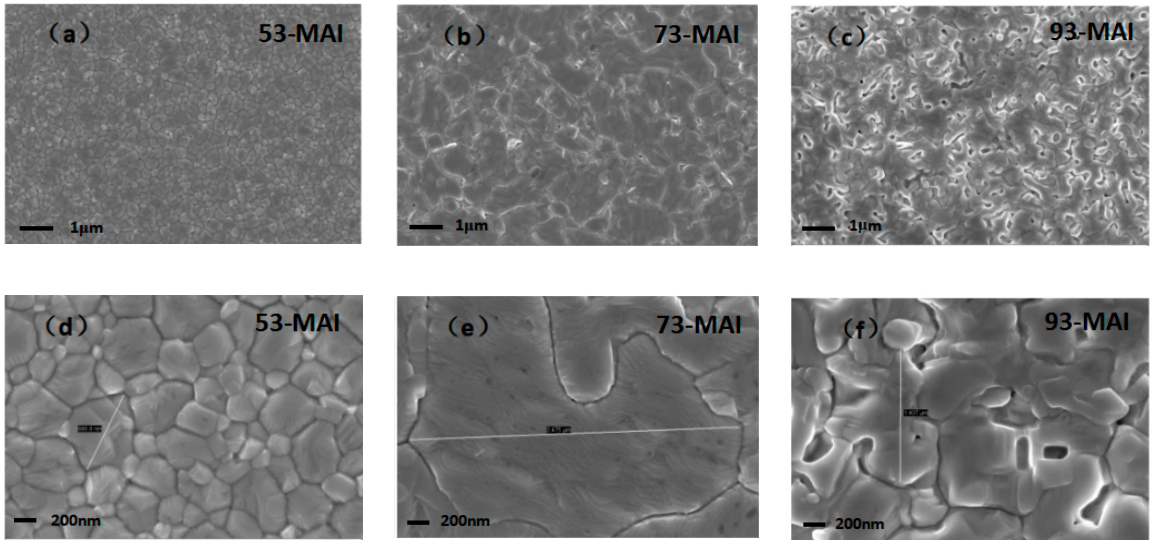

Figure 4. SEM top views of organic–inorganic hybrid perovskite films with different concentrations of CH_3NH_3I (MAI). The concentrations of (**a**–**c**) are 53 mg/mL, 73 mg/mL, and 93 mg/mL, respectively; (**d**–**f**) are enlarged views of (**a**–**c**).

The significant changes in the surface morphology (size and shape of grains) of perovskite films with different concentrations of MAI could be observed in SEM top views, which may be attributed to the growth state at the interface between the organic–inorganic hybrid perovskite layer and HTL. To explore the influence of the interface on the growth of perovskite, SEM cross-sectional views of light absorption layers prepared with different concentrations of MAI precursor solutions are shown in Figure 5a–c. Some bright spots (corresponding to the yellow circles) at the interface between the perovskite layer and NiO_x hole transport layer can be observed in Figure 5a, which may be the PbI_2 grains reacting incompletely [31]. A small amount of PbI_2 can act as an electron blocking layer, but huge grains may hinder the transport of holes [30]. When the concentration of MAI precursor solution is increased to 73 mg/mL, PbI_2 grains no longer exist at the interface, due to the complete reaction of MAI precursor solution and PbI_2 solution, which is conducive to transport of charge carrier. In Figure 5c, huge cracks in the perovskite layer and a significant transition of perovskite structure can be observed, indicating the deterioration of the morphology. In addition, the different thickness of perovskite films is observed with the increase in MAI concentration, which can affect not only the XRD peak intensity, but also the absorption and photoluminescence of the films.

By observing the SEM views, we find that the concentration of MAI precursor solution has a great influence on the surface morphology and structure of the organic–inorganic hybrid perovskite. Figure 6 shows the XRD pattern of perovskite with different concentrations of MAI precursor solution, and the annealing time of PbI_2 is 0 s. The diffraction peaks of (110), (211), and (220), appearing at $2\theta = 14.17°$, 23.6°, and 28.24°, can be found in the XRD pattern of MAI-53, corresponding to the cubic structure of perovskite shown in Figure 4d. The peak of (001) marked by diamond indicates the residual of PbI_2, which is consistent with SEM views. The enhanced intensity of the perovskite peaks can be seen from the pattern of MAI-73, which is owing to the increase in grain crystallinity and film thickness. As the

concentration increases, the PbI_2 peak disappears, and the splits of (002), (110), (004), and (220) peaks indicate the phase transition to a perfect tetragonal phase, corresponding to the morphology transition to tetragonal structure [31,32].

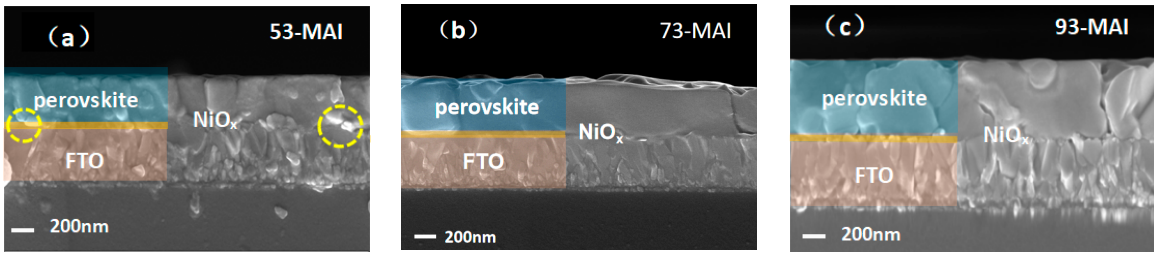

Figure 5. SEM cross-sectional views of organic–inorganic hybrid perovskite films with different concentrations of MAI precursor solution. (**a**–**c**) show the films with MAI concentrations of 53 mg/mL, 73 mg/mL, and 93 mg/mL, respectively.

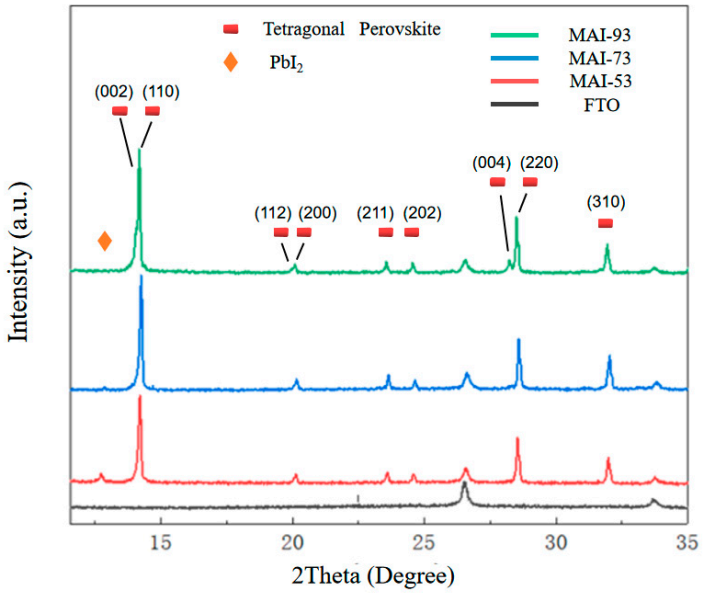

Figure 6. XRD patterns of perovskite films with different concentrations of MAI precursor solution.

In our work, the evolution of the organic–inorganic hybrid perovskite structure with the change of MAI concentration is observed. The cubic structure of perovskite is obtained with a low concentration of MAI, and the presence of residual PbI_2 at the interface can be found. When the concentration of precursor solution is 73 mg/mL, there is no significant change in perovskite composition. However, the decrease in PbI_2 peak proves the higher purity of perovskite formation. The grain size becomes larger and grain boundaries are not obvious, which indicates a transition trend of perovskite structure. With the increase in MAI solution, the growth of dendritic structure delivers the phase transition, deviating the perovskite toward tetragonal structure, which is also proved by the XRD patterns. In addition, there are no peaks of PbI_2 (corresponding to ~13°) and MAI (corresponding to ~19°) in the 93-MAI pattern, indicating the pure composition of perovskite, and the split of peaks (corresponding to ~14°and 28°) shows the perfect tetragonal phase of perovskite. The evolution processes of different samples are shown in Figure 7.

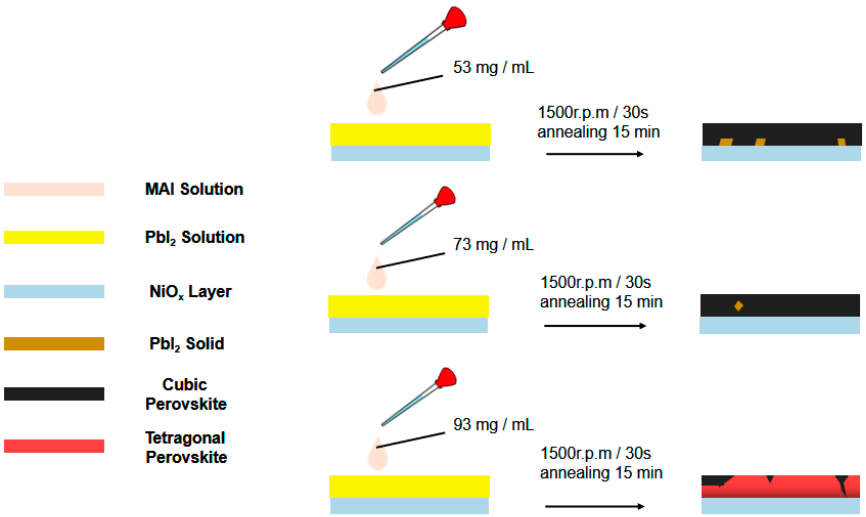

Figure 7. Evolution schematic diagram of organic–inorganic hybrid perovskite structure with different concentrations of MAI precursor solution.

The concentration of MAI also has great impact on the photophysical properties of the perovskite layer, which is reflected in the absorption and photoluminescence. Figure 8 shows the UV–Vis absorption spectra for organic–inorganic hybrid perovskite films with various concentrations of MAI precursor solutions, and the annealing time of PbI_2 is 0 s. The strong light absorption of all samples in the range of 450 nm to 750 nm can be observed from Figure 8, indicating the high crystallization quality of films deposited on unannealed PbI_2 bottom film. Moreover, the perovskite film of 73-MAI shows the strongest light absorption in the range of 650 nm to 750 nm, which is attributed to the improvement of perovskite crystallinity and increase in film thickness. As the concentration of the precursor solution increases, the red shift of the absorption edge can be observed from 790 nm to 806 nm, indicating the reduction of the band gap. It is speculated that the phase transition of perovskite structure with various concentration results in the narrower band gap of perovskite, which is beneficial to long wavelength absorption [33]. It is worth noting that the enhanced Urbach tail of absorption can be observed with the high degree of MAI concentration (corresponding to the orange circle in Figure 8). The result is similar to previous literature, which is ascribed to structural disorder with high degree of MAI solution [29]. The Urbach energy and steepness parameters are calculated, and listed in Table 1.

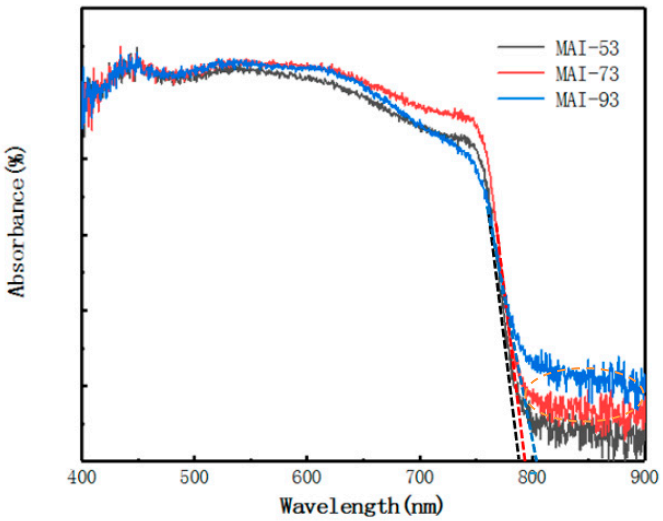

Figure 8. UV–Vis spectra of organic–inorganic hybrid perovskite films with different concentrations of MAI precursor solution.

Table 1. The Urbach energy and steepness parameters of absorption data.

MAI Concentration	Urbach Energy (meV)	Steepness Parameters
53 mg/mL	58.7	0.44
73 mg/mL	71.4	0.36
93 mg/mL	88.3	0.29

Organic–inorganic hybrid perovskite films are prepared on FTO/NiO_x substrates to measure the PL property. Figure 9 shows the PL spectra of perovskite films prepared by different concentrations of MAI precursor solution, and the annealing time of PbI_2 is 0 s. It can be seen that the emission peak of $MAPbI_3$ perovskite is located on around 770 nm. The reason for the high emission peak of sample MAI-53 is the blocking effect of PbI_2 grains on the transport of holes at the interface. The growth of perovskite crystals with moderate concentration of MAI results in less residual PbI_2 crystals and high-flatness perovskite film at the interface, which improves the capability of carrier extraction, and leads to the low emission peak intensity of MAI-73 sample. In addition, the inevitable photon re-absorption may occur in the lager thickness of perovskite film [26]. As the concentration increases, the intensity of the emission peak increases significantly. This abnormal enhancement is due to the phase transition of the perovskite structure. In addition, the full width at half maximum (FWHM) and emission peak center are measured, and listed in Table 2.

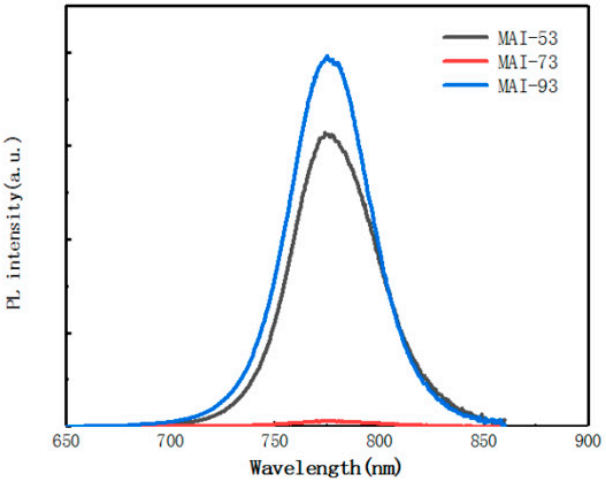

Figure 9. Photoluminescence spectra of organic–inorganic hybrid perovskite films with different concentrations of MAI precursor solution.

Table 2. The full width at half maximum (FWHM) and emission peak center of photoluminescence spectra.

Sample	FWHM (nm)	Emission Peak Center (nm)
MAI-53	47.3	675.6
MAI-73	45.3	677.9
MAI-93	46.9	674.4

The perovskite layer prepared with moderate concentration (73 mg/mL) of precursor solution has a transition trend to tetragonal structure. There is no remnant PbI_2 at the interface between the light absorbing layer and hole transport layer. In addition, the annealing time of the PbI_2 layer in this part of the experiment is the previously optimized processing time (0 s), ensuring the formed perovskite films are flat. The excellent morphology of perovskite films can be observed. Therefore, the better photophysical properties of the perovskite layer are obtained, which has laid the foundation for the preparation of high-performance perovskite solar cells and photodetectors.

4. Conclusions

In summary, the optimization of the preparing process (two-step method) for organic–inorganic hybrid perovskite film was investigated in our work. Firstly, the effect of PbI_2 annealing time on the film flatness of the perovskite was investigated. The deposition of MAI solution through liquid–liquid diffusion was more conducive to growing high-flatness perovskite film. In addition, various MAI concentrations were introduced to the preparation of the perovskite film. The enhanced absorption and carrier extraction capability of perovskite film were obtained with moderate MAI (73 mg/mL). A high degree of MAI concentration led to the transition of perovskite to typical tetragonal structure, resulting in the deterioration of film morphology.

The suitable annealing time of PbI_2 and concentration of MAI were determined in our experiments. Moreover, the optimization process for controlling the morphology and structure of perovskite was investigated. These results provide novel ideas to modulate the growth of $MAPbI_3$ crystal under the two-step method.

For the preparation of the inverted device, we just made a preliminary attempt by using processing techniques for the perovskite absorption layer. We will apply the optimization process for perovskite layer to the fabrication of device, and optimize the overall device to improve the power conversion efficiency.

Author Contributions: Z.Z.; X.Z.; J.Z.; J.C.; D.C.; C.C.; Y.Y.; X.Y.; H.R.; J.W.; B.L. and G.L. have read and agreed to the published version of the manuscript.

Funding: This research was funded by the project of the Natural Science Foundation of China (no. 61875186), the project of the Natural Science Foundation of Beijing (no. Z160002), the Key Research Projects of BISTU (2019KYNH227), and the Beijing Key Laboratory for Sensors of BISTU (no. 2019CGKF007).

Conflicts of Interest: The authors declare no conflict of interest.

References

1. Kojima, A.; Teshima, K.; Shirai, Y.; Miyasaka, T. Organometal halide perovskites as visible-light sensitizers for photovoltaic cells. *J. Am. Chem. Soc.* **2009**, *131*, 6050–6051. [CrossRef] [PubMed]
2. Lee, M.M.; Teuscher, J.; Miyasaka, T.; Murakami, T.N. Efficient hybrid solar cells based on meso-superstructured organometal halide perovskites. *Science* **2012**, *338*, 643–647. [CrossRef] [PubMed]
3. Li, X.; Bi, D.; Yi, C.; Decoppet, J.D. A vacuum flash-assisted solution process for high-efficiency large-area perovskite solar cells. *Science* **2016**, *353*, 58–62. [CrossRef] [PubMed]
4. Cho, K.T.; Paek, S.; Grancini, G.; Roldán-Carmona, C.; Gao, P.; Lee, Y.H.; Nazeeruddin, M.K. Highly efficient perovskite solar cells with a compositionally engineered perovskite/hole transporting material interface. *Energy Environ. Sci.* **2017**, *10*, 621–627. [CrossRef]
5. Zhao, Z.; Sun, W.; Li, Y.; Ye, S.; Rao, H.; Gu, F.; Liu, Z.; Bian, Z.; Huang, C. Simplification of device structures for low-cost, high-efficiency perovskite solar cells. *J. Mater. Chem. A* **2017**, *5*, 4756–4773. [CrossRef]
6. Han, T.H.; Tan, S.; Xue, J.; Meng, L.; Lee, J.W.; Yang, Y. Interface and defect engineering for metal halide perovskite optoelectronic devices. *Adv. Mater.* **2019**, *31*, 1803515. [CrossRef] [PubMed]
7. Filip, M.R.; Eperon, G.E.; Snaith, H.J.; Giustino, F. Steric engineering of metal-halide perovskites with tunable optical band, gaps. *Nat. Commun.* **2014**, *5*, 5757. [CrossRef]
8. Zhang, X.; Bi, S.; Zhou, J.; You, S.; Zhou, H.; Zhang, Y.; Tang, Z. Temperature-dependent charge transport in solution-processed perovskite solar cells with tunable trap concentration and charge recombination. *J. Mater. Chem. C* **2017**, *5*, 9376–9382. [CrossRef]
9. Azarhoosh, P.; McKechnie, S.; Frost, J.M.; Walsh, A.; Schilfgaarde, M.V. Research update: Relativistic origin of slow electron-hole recombination in hybrid halide perovskite solar cells. *APL Mater.* **2016**, *4*, 091501. [CrossRef]
10. Hsieh, C.M.; Liao, Y.S.; Lin, Y.R.; Chen, C.P.; Tsai, C.M.; Diau, E.W.G.; Chuang, S.C. Low-temperature, simple and efficient preparation of perovskite solar cells using Lewis bases urea and thiourea as additives: Stimulating large grain growth and providing a PCE up to 18.8%. *RSC Adv.* **2018**, *8*, 19610–19615. [CrossRef]

11. Jeon, N.J.; Noh, J.H.; Yang, W.S.; Kim, Y.C.; Ryu, S.C.; Seo, J.; Seok, S. Compositional engineering of perovskite materials for high-performance solar cells. *Nature* **2015**, *517*, 476–480. [CrossRef] [PubMed]
12. Wang, S.L.; Yang, F.; Zhu, J.R.; Cao, Q.X.; Zhong, Y.G.; Wang, A.C.; Du, W.N.; Liu, X.F. Growth of metal halide perovskite materials. *Sci. China Mater.* **2020**, *63*, 1438–1463. [CrossRef]
13. Docampo, P.; Hanusch, F.C.; Giesbrecht, N.; Angloher, P.; Ivanova, A.; Bein, T. Influence of the orientation of methylammonium lead iodide perovskite crystals on solar cell performance. *APL Mater.* **2014**, *2*, 081508. [CrossRef]
14. Wang, M.; Feng, Y.; Bian, J.; Liu, H.Z.; Shi, Y.T. A comparative study of one-step and two-step approaches for MAPbI 3 perovskite layer and its influence on the performance of mesoscopic perovskite solar cell. *Chem. Phys. Lett.* **2017**, *692*, 44–49. [CrossRef]
15. Pellet, N.; Gao, P.; Gregori, G.; Yang, T.Y.; Nazeeruddin, M.K.; Maier, J.; Gratzel, M. Mixed-organic-cation perovskite photovoltaics for enhanced solar-light harvesting. *Angew. Chem. Int. Ed.* **2014**, *53*, 3151–3157. [CrossRef] [PubMed]
16. Kim, H.S.; Im, S.H.; Park, N.G. Organolead halide perovskite: New horizons in solar cell research. *J. Phys. Chem. C* **2014**, *118*, 5615–5625. [CrossRef]
17. Chauhan, M.; Zhong, Y.; Schötz, K.; Tripathi, B.; Köhler, A.; Huettner, S.; Panzer, F. Investigating two-step MAPbI3 thin film formation during spin coating by simultaneous in situ absorption and photoluminescence spectroscopy. *J. Mater. Chem. A* **2020**, *8*, 5086–5094. [CrossRef]
18. Wang, Y.; He, J.; Chen, H.; Chen, J.S.; Zhu, R.D.; Ma, P.; Towers, A.; Lin, Y.; Gesquiere, A.J.; Wu, S.T.; et al. Ultrastable, highly luminescent organic–inorganic perovskite–polymer composite films. *Adv. Mater.* **2016**, *28*, 10710–10717. [CrossRef]
19. He, J.; Towers, A.; Wang, Y.N.; Yuan, P.; Jiang, Z.; Chen, J.S.; Gesquiere, A.J.; Wu, S.Y.; Dong, Y.J. In situ synthesis and macroscale alignment of CsPbBr3 perovskite nanorods in a polymer matrix. *Nanoscale* **2018**, *10*, 15436–15441. [CrossRef]
20. He, Z.; Zhang, C.; Dong, Y.J.; Wu, S.-T. Emerging perovskite nanocrystals-enhanced solid-state lighting and liquid-crystal displays. *Crystals* **2019**, *9*, 59. [CrossRef]
21. Shahiduzzaman, M.; Hamada, K.; Yamamoto, K.; Nakano, M.; Karakawa, M.; Takahashi, K.; Taima, T. Thermal control of PbI_2 film growth for two-step planar perovskite solar cells. *Cryst. Growth Des.* **2019**, *19*, 5320–5325. [CrossRef]
22. Gao, H.; Meng, X.; Du, Y.L.; Gao, X.Y. Fabrication and characterization of perovskite CH_3NH_3PbI_3 films via two-step sol-gel process: Impact of soaking time of PbI_2. *Thin Solid Films* **2019**, *682*, 37–43. [CrossRef]
23. Jia, F.J.; Guo, Y.Q.; Che, L.J.; Liu, Z.Y.; Zeng, Z.G.; Cai, C.B. Synergic solventing-out crystallization with subsequent time-delay thermal annealing of PbI_2 precursor in mesostructured perovskite solar cells. *Mater. Res. Express* **2018**, *5*, 066404. [CrossRef]
24. Ling, T.; Zou, X.P.; Cheng, J.; Bai, X.; Ren, H.Y.; Chen, D. Modified sequential deposition route through localized-liquid-liquid-diffusion for improved perovskite multi-crystalline thin films with micrometer-scaled grains for solar cells. *Nanomaterials* **2018**, *8*, 416. [CrossRef]
25. Im, J.H.; Jang, I.H.; Pellet, N.; Grarzel, M.; Park, N.G. Growth of CH3NH3PbI3 cuboids with controlled size for high-efficiency perovskite solar cells. *Nat. Nanotechnol.* **2014**, *9*, 927–932. [CrossRef]
26. Sun, X.G.; Shi, Z.F.; Li, Y.; Lei, L.Z.; Li, S.; Wu, D.; Xu, T.T.; Tian, Y.T.; Li, X.J. Effect of CH_3NH_3I concentration on the physical properties of solution-processed organometal halide perovskite $CH_3NH_3PbI_3$. *J. Alloys Compd.* **2017**, *706*, 274–279. [CrossRef]
27. Chen, L.C.; Lee, K.L.; Wu, W.T.; Hsu, C.F.; Tseng, Z.L.; Sun, X.H.; Kao, Y.T. Effect of different CH3NH3PbI3 Morphologies on photovoltaic properties of perovskite solar cells. *Nanoscale Res. Lett.* **2018**, *13*, 140. [CrossRef]
28. Fu, Y.; Meng, F.; Rowley, M.B.; Thompson, B.J.; Shearer, M.J.; Ma, D.; Hamers, R.J.; Wright, J.C.; Jin, S. Solution growth of single crystal methylammonium lead halide perovskite nanostructures for optoelectronic and photovoltaic applications. *J. Am. Chem. Soc.* **2015**, *137*, 5810–5818. [CrossRef]
29. Acuna, D.; Krishnan, B.; Shaji, S.; Avellaneda, D. On the structure and physical properties of methyl ammonium lead iodide perovskite thin films by the two-step deposition method. *Mater. Chem. Phys.* **2018**, *215*, 137–147.
30. Zhao, Y.C.; Li, Q.; Zhou, W.K.; Hou, Y.; Zhao, Y.; Fu, R. Double-side-passivated perovskite solar cells with ultra-low potential loss. *Solar RRL* **2019**, *3*, 1800296. [CrossRef]

31. Zhu, H.; Fu, Y.; Meng, F.; Wu, X.X.; Gong, Z.Z.; Ding, Q.; Gustafsson, M.V.; Trinh, M.T.; Jing, S.; Zhu, X.Y. Lead halide perovskite nanowire lasers with low lasing thresholds and high quality factors. *Nat. Mater.* **2015**, *14*, 636–642. [CrossRef] [PubMed]
32. Liang, K.; Mitzi, D.B.; Prikas, M.T. Synthesis and characterization of organic−inorganic perovskite thin films prepared using a versatile two-step dipping technique. *Chem. Mater.* **1998**, *10*, 403–411. [CrossRef]
33. Tang, Z.; Bessho, T.; Awai, F.; Kinoshita, T.; Maitani, M.; Jono, R.; Murakami, T.; Wang, H.; Kubo, T.; Uchida, S.; et al. Hysteresis-free perovskite solar cells made of potassium-doped organometal halide perovskite. *Sci. Rep.* **2017**, *7*, 12183. [CrossRef] [PubMed]

© 2020 by the authors. Licensee MDPI, Basel, Switzerland. This article is an open access article distributed under the terms and conditions of the Creative Commons Attribution (CC BY) license (http://creativecommons.org/licenses/by/4.0/).